

Diocotron Instabilities in an Electron Column Induced by a Small Fraction of Transient Positive Ions

Andrey A. Kabantsev and C. Fred Driscoll

Physics Department, University of California at San Diego, La Jolla CA 92093-0319 USA

Abstract. It is well known that a small fraction of positive ions can destabilize diocotron modes on electron plasmas. However, the historical (and recent) interpretation of experimental results in terms of 2D (or modified 2D) theories of ion-induced instabilities is apparently erroneous. Here, we experimentally characterize a strong exponential instability with no threshold, obtaining growth rates orders of magnitude larger than predicted. The positive ion population is maintained either by continuous external injection of ions or by ionization of the background gas within hot electron plasmas. In both cases, the observed exponential growth rate γ_m is directly proportional to the ion creation rate ν_+ , i.e., $\gamma_m = \kappa_m \nu_+$, with $\kappa_m \approx (10^1-10^3)/N_e$ for $m_\theta = 1, 2, 3$. Experimental results also suggest that non-2D effects, including end confinement fields, are important. This strong instability may have important implications for the anti-hydrogen creation technique of propelling anti-protons through trapped e^+ clouds.

INTRODUCTION

Theory demonstrates that two-component nonneutral plasmas consisting of trapped electrons and a small fraction of ions can exhibit unstable $k_z = 0$ diocotron modes if there is a resonance between the electron diocotron modes and the radial motion of the ion [1]. This *exponential* ion-resonance instability [2] was suspected to be the dominant loss mechanism in toroidal experiments [3,4]. This original analysis [2] treated the case of trapped ions; the case of untrapped (transient) ions was investigated later in a linear electron trap configuration both experimentally [5] and theoretically [6]. Several significant differences were found between these two cases: transient ions appeared to cause *linear* rather than *exponential* growth; and this linear growth occurs over a somewhat broader region around the resonance.

The 2D-analysis of non-resonant motion of transient ions in an electron column by Fajans [6] suggests that the average ion motion is well represented by the orbit of an ion which is placed initially at the electron column center. This “average ion” orbits around a fixed point in the $m_\theta = 1$ diocotron frame, and this point is displaced *outward* from the center of electron column by a small distance Δ , which is a small fraction of the diocotron mode amplitude D , i.e., $\Delta \sim (r_p^4/\lambda)D$. Here, $r_p \equiv R_p/R_w$ is the electron column radius, and the ion magnetization parameter [2] is $\lambda \equiv B^2/2\pi n_e m_i c^2 \gg 1$. An ion wobbling around this fixed point causes an exponential

growth of the diocotron mode, with a rate which can be derived from Eq. 24 in Ref. 6 as $\gamma_1^{th} \approx \nu_+ r_p^4 / (1 - r_p^2) \lambda$. Here, ν_+ is the ion production (internal ionization or external injection) rate per trapped electron. Thus, one expects growth rates much less than the ion production (injection) rate, i.e., $\gamma_1^{th} / \nu_+ \ll 1$.

However, our measurements of γ_1 and ν_+ in the range of $10^{-5} \leq r_p^4 / \lambda \leq 10^{-2}$ show that $\gamma_1 / \nu_+ \gg 1$, which suggests a process not treated in prior analysis. In particular, this result implies that the lifetime-averaged displacement of the ion exceeds the diocotron radius D by factor of 10^1 - 10^3 even far away from the resonance.

Since many of the current experiments on a cold antihydrogen production require the propulsion of antiprotons through the trapped positron plasma [7,8], there is a free energy to drive similar instabilities. Due to slow antihydrogen formation rates, even weak instabilities could be troublesome. Here, we find that instabilities essentially always occur, with growth rates proportional to the number of transiting ions.

EXPERIMENTAL SETUP

Our experiments are performed in a cylindrical Penning-Malmberg trap, as shown schematically in Fig. 1. The electron column of length $L_p \leq 50$ cm is contained inside a stack of hollow conducting cylinders of radius $R_w = 3.5$ cm, which reside in an ultrahigh vacuum with residual pressure $P \approx 0.1$ nTorr. Molecular hydrogen from the warm walls is a majority (95%) of the background neutral gas. The end cylinders G_1 and G_{10} are negatively biased, with $V_c \geq -100$ V, thereby providing axial confinement for the electrons. A strong axial magnetic field $B \leq 14$ kG ensures radial confinement both for the electrons and ions.

The electron column is generated by thermoionic emission from a hot tungsten filament located axially outside of the trapping region. Temporarily grounding the confinement gate G_1 allows the electrons to fill the trap. The resulting trapped electron column has typical density $1 \leq n_e \leq 2 \times 10^7$ cm⁻³ over a bell-shaped radial profile with a characteristic radius $R_p \approx 1.2$ cm, and with temperature $0.6 \leq T_e \leq 0.8$ eV before auxiliary heating. The electrons can be heated by applying short (≤ 5 ms) rf-burst of variable amplitude and tuned frequency to one of the end confining cylinders in resonance with the particles bounce motion [9].

In our experiments we generate ions by ionization of the background gas directly inside the electron column, or by continuous injection of ions created by filament electrons in the Grid- G_1 region. In both cases, the resulting fluxes of ions are directly proportional to the background neutral pressure. The beam method has the advantage of independence of the electron plasma temperature, which is especially important at high pressures due to ionization cooling. The rf-heating method has the advantage of allowing direct measurement of the ionization rate simultaneously with the mode growth rate: since every ionization adds one electron to the plasma column, the ionization rate follows directly from the charge accumulation rate (if ions are not confined in the trap).

The growth rates $\gamma_m(t)$ for the $k_z = 0$, $m_\theta = 1, 2, 3, \dots$ diocotron modes are measured by digitizing the amplitudes $A_m(t)$ of corresponding wall signals induced by the diocotron oscillations at the sector electrodes S_4 and S_7 . These amplitudes are

verified (and calibrated) by calculating the center-of-mass displacement D (or the quadrupole moment Q for the $m_\theta = 2$ case) of the dumped plasma column from CCD camera diagnostic [10]. The ionization rate $\nu_+(t)$ is obtained *simultaneously* with $\gamma_m(t)$, by measuring the frequency change of the $m_\theta = 1$ diocotron mode; that is, $\nu_+ = (1/N_e)dN_e/dt = (1/f_1)df_1/dt$, with verification by the relative change in the total number of electrons dumped onto the phosphor screen. In the experiments, we keep the scaled mode amplitudes, $d \equiv D/R_w$, small enough ($d \leq 0.03$) to keep nonlinear effects [11] in the mode frequency ($\delta f_1/f_1 \leq d^2$) well below the resolution level of our frequency measurements (0.01%).

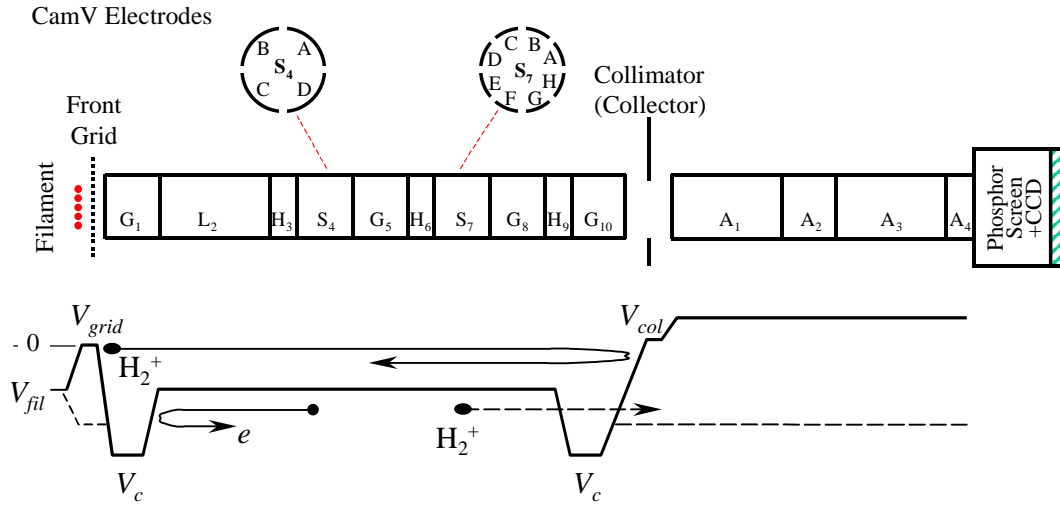


FIGURE 1. Cylindrical Penning-Malmberg trap and imaging diagnostics, with potential profiles for two configurations: a double-well configuration with axially *trapped* ions (solid); and a single-well configuration with *transient* ions (dashed).

ENERGETIC ION INJECTION

Figure 2 shows the ion current i_+ transiting through the electron column as a function of the neutral pressure when ions are not trapped at the dump end of the trap. In this particular case, the front grid was positively biased, $V_{grid} = +10$ V, and the filament was at $V_{fil} = -40$ V. Thus, the maximum energy acquired by emitted electrons near the grid, $\mathcal{E}_{max} = V_{grid} - V_{fil} \approx 50$ eV, was close to the energy providing the maximum of the ionization cross-section for molecular hydrogen. The ion current is measured at the collector plate put temporarily behind the end confining cylinder G_{10} . One can see a linear dependence $i_+(P_{H_2})$, with an offset probably due to ionization of gases desorbed from the grid surface; the pressure is measured 1m distant from the confinement electrodes.

Figure 3 shows the ion current as a function of the electron energy \mathcal{E}_{max} for two extreme pressures. Thus, we have an adjustable source of transient ions; the current can be easily controlled over a vast range by the front grid bias, or by the background neutral pressure.

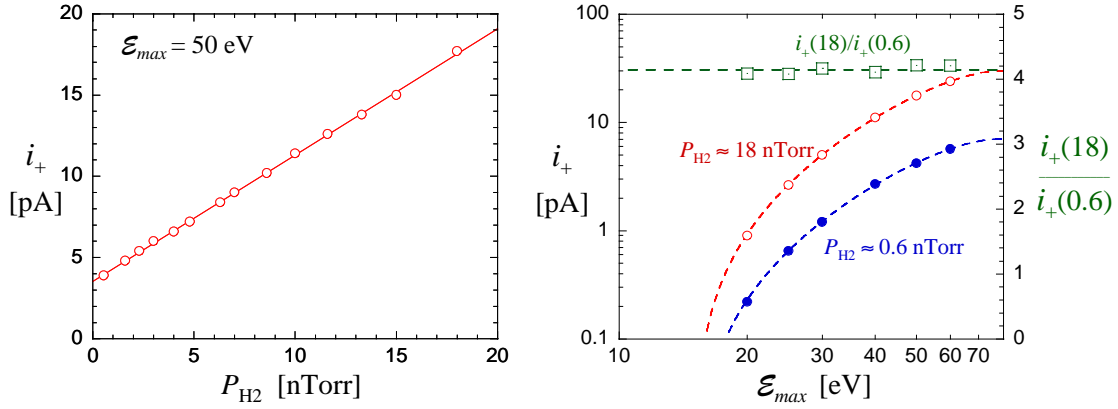


FIGURE 2. The ion current from ionization in the Grid-G₁ region versus neutral pressure.
FIGURE 3. The ion current versus the maximum beam energy \mathcal{E}_{max} for two neutral pressures, and their ratios.

If we apply a potential to the collector plate, which is more positive than the potential at the front grid, then this continuously injected flow of ions gets trapped between the grid and the collector plate. Trapped ions bounce back and forth through the electron column, causing an even greater instability of the diocotron modes. Typical dependencies of the instability growth rates γ_m on neutral pressure are shown in Fig. 4 for $m_\theta = 1, 2$. The growth rates are linearly proportional to the neutral pressure (i.e., to the ion current) over two orders of magnitude. Here, we have subtracted the zero-current growth (or damping) rate $\gamma_m(0)$, arising from resistive instability and asymmetry-induced damping. For these conditions, $\gamma_1(0) = +0.24 \text{ s}^{-1}$ and $\gamma_2(0) = -0.081 \text{ s}^{-1}$. Higher m_θ -modes show even greater instability rates, but they rapidly develop non-linear saturation due to spatial Landau damping in the radial edge of the plasma column. Hence, we focus predominantly on the basic ($m_\theta = 1$) diocotron mode.

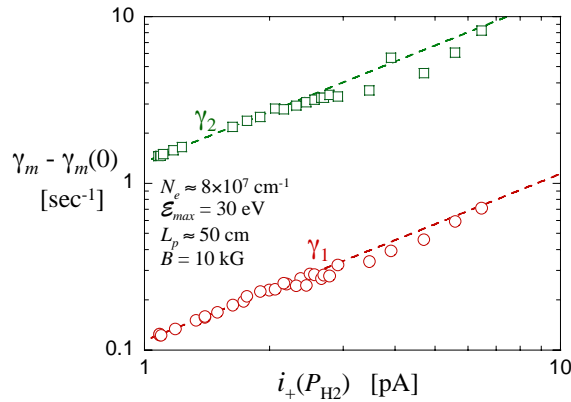


FIGURE 4. The instability growth rates versus (continuously injected) ion current in the double-well configuration.

Modulating the energy of electron beam or the ion trapping potential modulates the flux of trapped ions, and this correspondingly modulates the growth rates γ_m , as shown

in Figs. 5a,b. Opening a confinement gate for the trapped ions (by decreasing the bias V_{col} on the collector plate below the plasma potential) causes an immediate and dramatic effect: the growth rate goes down more than 10 times. Re-establishing ion trapping causes linear growth in γ_1 , due to increase in number of ions, limited by an “active time” $\tau_a \sim 0.1$ s. We believe that τ_a represents the time required for ions to move radially to the edge of electron column. This active lifetime shows an approximate empirical scaling $\tau_a \propto B/V_c L_c$, which suggests $\mathbf{E} \times \mathbf{B}$ θ -drift nature. Here, V_c is the electron confinement voltage applied to the end cylinders, and L_c is the length of those cylinders at V_c . This probably arises from $\delta\theta \propto V_c L_c$ as the relative θ -drift of the ions with respect to the phase of the electron column diocotron rotation.

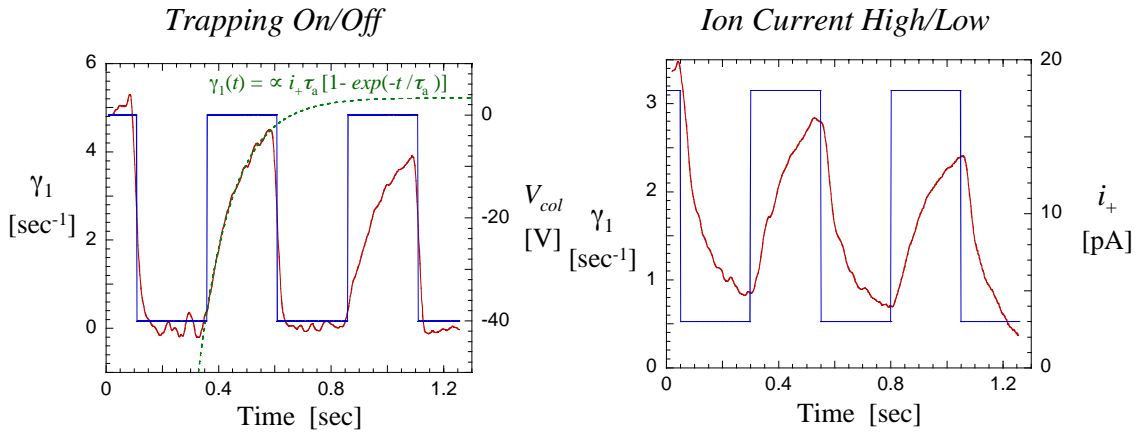


FIGURE 5. Growth rates with square-wave modulated trapping (left) and injection current (right) of the ions.

Note that while the growth rate $\gamma_1(t)$ shows an exponential saturation due to τ_a of the trapped ions, the fractional neutralization $\alpha(t) \equiv N_i/N_e = \nu_+ t$ grows linearly due to continuous trapping of injected ions. Thus, at high enough values of $i_+(P_{H2})$, the “ionization rate” ν_+ can be directly measured from the linear decrease in the diocotron frequency $f_1(t)$ due to continuous accumulation of the ion space charge (most likely, at the periphery of electron column), i.e., $f_1(t) \propto N_e(1 - \nu_+ t)$, and hence, $\nu_+ \approx -(1/f_1)df_1/dt$.

Figure 6 demonstrates that the observed decrease in the diocotron frequency $f_1(t)$ is indeed due to the trapping and accumulation of positive ions: after letting them go away at $t = 6.6$ s, the diocotron frequency immediately rises up to its initial value simultaneously with a halt in the mode growth (the 5 Hz steps in f_1 are instrumental only).

Taking data similar to Fig. 6 at different values of $i_+(P_{H2})$, we can plot the corresponding growth rates γ_1 versus $\nu_+ = i_+/Q_e$. The best linear fit gives us the ratio $\gamma_1/\nu_+ \approx 400$. In general, we find that this non-resonant ion-induced instability shows exponential growth with a rate γ_1 directly proportional to the “ionization rate” $\nu_+ = i_+/Q_e$, and that $\gamma_1/\nu_+ \gg 1$ in the whole range of $\lambda(B) \gg 1$.

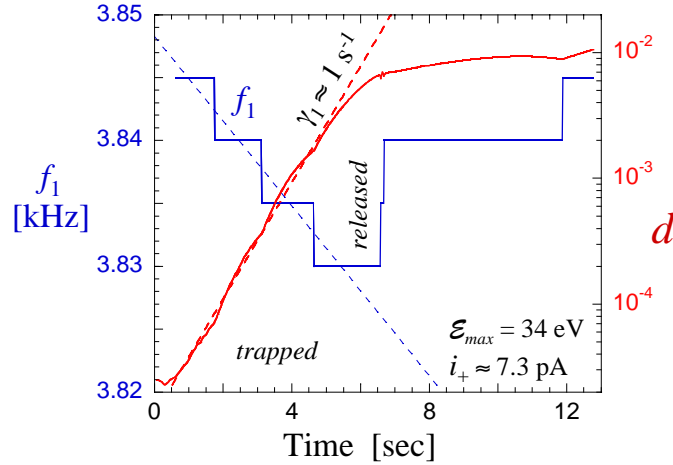


FIGURE 6. Temporal behavior of the diocotron mode frequency f_1 and its amplitude d with trapping and release in double-well configuration.

IN-PLACE IONIZATION

Another approach to this problem of the non-resonant ion-induced instabilities lies in ionization of background neutrals directly in an electron column. To get the ionization rate at measurable level we raise T_e up to 7-9 eV with rf-heating burst. In this experimental configuration, each ion freely escapes from the trap in a time $\tau_i \sim L_p/v_i \leq 1$ ms, leaving its counterpart electron inside the trap. Therefore, the electron column image charge and the diocotron frequency have an increase proportional to $v_+(t)$, so we can obtain the ionization rate as $v_+(t) \equiv 1/f_1 df_1/dt$.

Figures 7a and 7b show typical evolutions of this calculated ionization rate $v_+(t)$ and the diocotron mode amplitude $d(t)$ after heating at $t_0 = 4.6$ s. At the low pressure of Fig. 7a, v_+ remains essentially constant after the heating burst, and d growth exponentially. At the higher pressure of Fig. 7b, electron cooling causes v_+ to decrease with time, and a surprisingly *linear* growth of d is observed. However, this represents the same exponential instability, i.e., $\partial d/\partial t = \kappa_1 v_+(t) d$, but with a rapidly decreasing v_+ . This can be seen directly from the $d(t)$ and $f_1(t)$ data, since $\kappa_1 \equiv \gamma_1/v_+ = \partial \ln(d/d(t_0)) / \partial \ln(f_1/f_1(t_0))$. Figure 8 shows a slope $\kappa_1 \approx 20$ for all time, demonstrating that the surprising linear growth of d is an insignificant consequence of electron cooling causing $v_+(t)$ to decrease.

Thus, we have got again a definitive evidence that $\gamma_1 = \kappa_1 v_+$, where $\kappa_1 \approx 20$. Adding double-well potential to the ends makes these ions temporarily trapped, and we then observe an additional twenty-fold increase in κ_1 , which brings it close to the typical level for the ion injection case ($\kappa_1 \sim 400$). The ions have a finite residence time τ_i (depending on v_{zi}), and the growth rate depends on $\kappa_1(\tau_i)$. Note that a typical fractional neutralization for this case of in situ ionization is $\alpha(t) = v_+(t)\tau_i \ll 10^{-4}$.

The instability factor κ_1 shows a surprising sensitivity (factor of two) to the plasma column shape $n(r, z)$. It is hard to quantify this dependence experimentally. However, we have observed a good correlation between the κ_1 dependence on the radial density profile and a factor of “excitability” of the $m_\theta = 1$ diocotron mode from a wall sector.

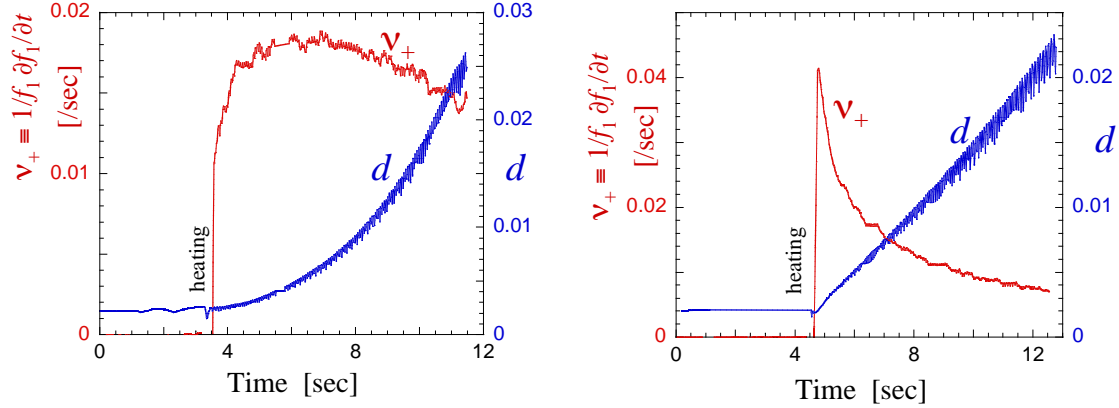


Figure 7. Temporal behavior of the ionization rate v_+ and the $m_\theta = 1$ diocotron mode amplitude d in single-well configuration. Left figure shows simple exponential growth with nearly constant $v_+(t)$ at low pressure $P_{H_2} \approx 0.5$ nTorr. Right figure shows *quasi-linear* growth due to strongly decreasing $v_+(t)$ caused by the fast cooling at higher pressure $P_{H_2} \approx 2$ nTorr.

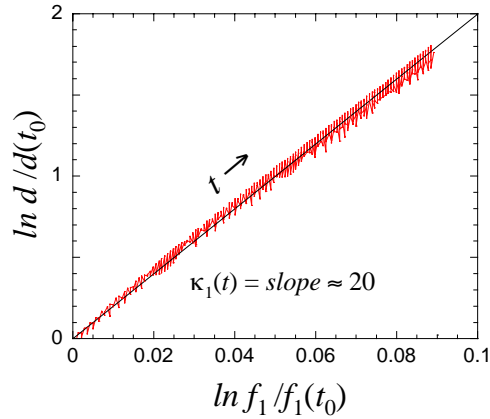


Figure 8. Exponential instability (Fig. 7b) with decreasing $\gamma_1(t) \approx 20 v_+(t)$. The slope $\kappa_1 \equiv \gamma_1/v_+ = \partial \ln(d/d(t_0)) / \partial \ln(f_1/f_1(t_0))$ is nearly constant for all time.

This plasma column shape is also sensitive to the magnetic field through transport processes. Due to these reasons, the growth rate scaling with magnetic field is not well established. Nevertheless, our preliminary measurements within close plasma shapes show a scaling consistent with $\gamma_1 \propto B^{0 \pm 0.2}$ in the range $2 \leq B \leq 14$ kG. This result is also in apparent contradiction to the $1/B^2$ magnetic scalings predicted by the 2D-theories of the ion-induced instabilities [2,6].

CONCLUSIONS

Diocotron instabilities are commonly observed when ions are present in pure electron plasmas [3-5,12]. Here, we establish an exponential growth of diocotron modes $m_\theta = 1, 2, 3$ with growth rates γ_m that are directly proportional to the incoming ion rates v_+ , and with corresponding coefficients $\kappa_m \equiv \gamma_m / v_+$ that are orders of magnitude greater than one. These effects may have strong implications for a variety

of experiments that propel bunch of ions many times through an electron/positron cloud [7,8].

The present results show that the existing 2D-theory of the transient ion instability underestimates the growth rate by many orders of magnitude, and indicates that as-yet-unspecified non-2D effects play a dominant role in ion motion. One possible candidate for this effect is the difference between the bounce-averaged rotation frequencies of electrons and ions; this difference comes from the two species sampling somewhat different radial electric fields at the plasma ends (the so called the magnetron rotation). This basic effect has been incorporated in several theory approaches [12,13]; but these theories show little correspondence to the present experimental results.

Broadly, it appears that azimuthal drift of electrons and ions tends to polarize the diocotron mode density perturbations, thereby developing instability similar to the classical flute MHD-instability of neutral plasmas confined in non-uniform magnetic fields. Moreover, the observed dependencies of growth rate on the confinement voltage and on the plasma column length are generically consistent with this hypothesis.

ACKNOWLEDGMENTS

This work was supported by NSF grant PHY-9876999.

REFERENCES

1. Davidson, R.C., *Physics of Nonneutral Plasmas*, Redwood Addison-Wesley, 1990, pp. 260-264.
2. Levy, R. H., Daugherty, J.D., and Buneman, O., *Phys. Fluids* **12**, 2616-2629 (1969).
3. Daugherty, J.D., Eninger, J.E., and Janes, G.S., *Phys. Fluids* **12**, 2677-2693 (1969).
4. Clark, W., Korn, P., Mondelli, A., and Rostoker, N., *Phys. Rev. Letters* **37**, 592-595 (1976).
5. Perrung, A.J., Notte, J., and Fajans, J., *Phys. Rev. Letters* **70**, 295-298 (1993).
6. Fajans, J., *Phys. Fluids* **B 5**, 3127-3135 (1993).
7. Amoretti, M., Bonomi, G., Bouchta, A., *et al.*, *Phys. Plasmas* **10**, 3056-3064 (2003).
8. Gabrielse, G., Bowden, N.S., Oxley, P., *et al.*, *Phys. Rev. Letters* **89**, 213401(4) (2002).
9. Beck, B.R., Fajans, J., and Malmberg, J.H., *Phys. Rev. Letters* **68**, 317-320, 1992).
10. Fine, K.S., Flynn, W.G., Cass, A.C., and Driscoll, C.F., *Phys. Rev. Letters* **75**, 3277-3280 (1995).
11. Fine, K.S., Driscoll, C.F., and Malmberg, J.H., *Phys. Rev. Letters* **63**, 2232-2235 (1989).
12. Pasquini, T., and Fajans, J., *Bull. Am. Phys. Society* **47**(9), 127 (2002).
13. Hilsabeck, T.J., and O'Neil, T.M., *Workshop on NNP 2001*, Abstracts (2001).